Collective states and charge density waves in the group IV transition metal trichalcogenides ©

Cite as: Appl. Phys. Lett. **118**, 210502 (2021); https://doi.org/10.1063/5.0052295 Submitted: 30 March 2021 • Accepted: 11 May 2021 • Published Online: 27 May 2021

🗓 M. D. Randle, 🗓 A. Lipatov, I. Mansaray, et al.

COLLECTIONS

Paper published as part of the special topic on Charge-Density-Wave Quantum Materials and Devices



This paper was selected as Featured







ARTICLES YOU MAY BE INTERESTED IN

Myths and truths about optical phase change materials: A perspective Applied Physics Letters 118, 210501 (2021); https://doi.org/10.1063/5.0054114

Distinctive features of the charge density wave collective motion driven by Hall electric field in NbSe₃

Applied Physics Letters 118, 213102 (2021); https://doi.org/10.1063/5.0051438

Evidence for a thermally driven charge-density-wave transition in 1T-TaS₂ thin-film devices: Prospects for GHz switching speed

Applied Physics Letters 118, 093102 (2021); https://doi.org/10.1063/5.0044459





Collective states and charge density waves in the group IV transition metal trichalcogenides ()

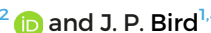
Cite as: Appl. Phys. Lett. 118, 210502 (2021); doi: 10.1063/5.0052295 Submitted: 30 March 2021 · Accepted: 11 May 2021 · Published Online: 27 May 2021







M. D. Randle, 🕩 A. Lipatov, 🕩 I. Mansaray, J. E. Han, A. Sinitskii, 🕩 and J. P. Bird 🗀 🕞



AFFILIATIONS

- Department of Electrical Engineering, University at Buffalo, Buffalo, New York 14260, USA
- ²Department of Chemistry, University at Nebraska-Lincoln, Lincoln, Nebraska 68588, USA

Note: This paper is part of the APL Special Collection on Charge-Density-Wave Quantum Materials and Devices.

a) Author to whom correspondence should be addressed: jbird@buffalo.edu

ABSTRACT

It has been nearly a century since the original mechanism for charge density wave (CDW) formation was suggested by Peierls. Since then, the term has come to describe several related concepts in condensed matter physics, having their origin in either the electron-phonon or electron-electron interaction. The vast majority of CDW literature deals with systems that are metallic, where discussions of mechanisms related to the Fermi surface are valid. Recently, it has been suggested that semiconducting systems such as TiS₃ and TiSe₂ exhibit behavior related to CDWs. In such cases, the origin of the behavior is more subtle and intimately tied to electron-electron interactions. We introduce the different classifications of CDW systems that have been proposed and discuss work on the group IV transition metal trichalcogenides (TMTs) (ZrTe₃, HfTe₃, TiTe₃, and TiS₃), which are an exciting and emergent material system whose members exhibit quasi-onedimensional properties. TMTs are van der Waals materials and can be readily studied in the few-layer limit, opening new avenues to manipulating collective states. We emphasize the semiconducting compound TiS3 and suggest how it can be classified based on available data. Although we can conjecture on the origin of the CDW in TiS3, further measurements are required to properly characterize it.

Published under an exclusive license by AIP Publishing. https://doi.org/10.1063/5.0052295

I. INTRODUCTION

The concept of a charge density wave (CDW) originates from Peierls' work, which identified the fundamental instability of a metallic one-dimensional (1D) atomic chain at zero temperature. It was found that a lattice reconstruction is energetically favorable under the influence of an electronic disturbance having k-space periodicity equal to twice the Fermi wavevector ($\mathbf{q} = 2\mathbf{k}_{\mathrm{F}}$). For a half-filled band, the reconstruction is accompanied by a metal-insulator transition. The term CDW itself was coined by Fröhlich² around the same time in his description of a 1D superconductor, which carried current by a collective charge transport mechanism, i.e., a CDW. In real systems, the CDW does not carry current without resistance, but rather is influenced by various pinning mechanisms. This leads to a description of conduction in which the CDW can only contribute to the current after overcoming a critical depinning field.³ The currently accepted model of CDW transport was developed some 20 years later by Fukuyama, Lee, and Rice over the course of several seminal papers. 4-6 It describes a classical picture where the CDW is modeled as an elastic object that interacts with randomly distributed impurity centers in order to

minimize its energy. Extensions to this model have been developed to further understand the nature of CDW depinning. The general description coming from this model provides the basis for many simulations and attempts to fit experimental data in a variety of quasi-1D systems. In the mean-field theory of CDWs, 10,111 the CDW state is stabilized only below a certain temperature (T_{CDW}) because the 2 k_F phonon mode becomes increasingly screened as temperature increases, eventually quenching the CDW state. 10 Since long-range order is not realizable at finite temperatures, 12 the existence of a CDW transition in real materials requires refinements to the mean-field theory. Explicitly, the inclusion of thermodynamic fluctuations, which can be suppressed by interchain coupling, results in lower estimates for T_{CDW} than in the mean-field theory. 12,1

The transition metal trichalcogenides (TMTs) are a particular class of quasi-1D linear-chain compounds that have been extensively studied in the context of CDWs. A recent resonant x-ray diffraction (XRD) experiment on the group IV TMT ZrTe₃ has indicated the importance of disorder in solidifying long-range order in practical CDW systems. Explicitly, it has been suggested that Friedel oscillations

³Department of Physics, University at Buffalo, Buffalo, New York 14260, USA

are key in stabilizing the CDW.¹⁴ Interestingly, the importance of Friedel oscillations was suggested in some of the earliest models of CDW transport.¹⁵ Indeed, Friedel oscillations have been imaged in the blue bronzes¹⁶ and in NbSe₃.¹⁷ Clearly, the advent of more advanced spectroscopic and microscopic techniques allows us to expand upon these older ideas and determine the true nature of collective state formation in a wide variety of material systems. We discuss several CDW materials in this article, with an emphasis on the group IV TMTs. A summary of selected properties of these materials can be found in Table I.

Many different systems show evidence of CDW formation, and often their behavior cannot be straightforwardly linked to Peierls' original model. In fact, it has been shown that only a very limited set of systems truly exhibit behavior analogous to what Peierls described. Recently, a classification system has been suggested in order to correct many of the misconceptions in the field. In short, it has been argued that there are at least three different classes of CDW. Type I is due to the Peierls' instability, generalized to quasi-1D systems by the Fermi surface nesting (FSN) mechanism. In type II materials, CDW formation is attributed to a strong enhancement of electron–phonon coupling at a specific wavevector, albeit one unrelated to any obvious nesting condition. Finally, and in contrast to the type I and II mechanisms, type III CDWs are driven by electron–electron interactions in systems where the Coulomb energy dominates the total energy.

The essential physics and the origin of the type I and II CDWs comes from a model in which the free-electron gas is allowed to couple to the lattice, such as the one originally developed by Fröhlich.² This model yields a relationship between the unperturbed phonon spectrum and a renormalized version under the influence of various coupling mechanisms between the lattice and electron gas,

$$\omega(\mathbf{q})^2 = \omega_0(\mathbf{q})^2 + 2\omega_0(\mathbf{q})|g(\mathbf{q})|^2 \Re{\{\chi(\mathbf{q},\omega)\}}.$$
 (1)

Here, $g(\mathbf{q})$ represents the coupling strength between electronic states at \mathbf{k} and \mathbf{k}' with a corresponding phonon of wavevector $\mathbf{q} = \mathbf{k} - \mathbf{k}'$, and $\chi(\mathbf{q}, \omega)$ is the Lindhard response function. In the context of Eq. (1), type I CDWs arise from the particular structure of $\chi(\mathbf{q}, \omega)$ in lower dimensions, ¹¹ where the response of the electron

density is found to be divergent at the wavevector $\mathbf{q}=2\mathbf{k_F}$. Conversely, type II CDWs are associated with a strong enhancement of electron–phonon coupling [large g (\mathbf{q}) near a specific phonon wavevector \mathbf{q}]. In either case, the coupling leads to a softening of the phonon spectrum in the vicinity of \mathbf{q} . If this softening is strong enough to completely suppress the phonon mode, a lattice reconstruction occurs. This is known generically as the Kohn anomaly.²¹

As experimental capabilities increase, it is becoming more evident that very few systems exhibit true type I behavior. NbSe₃ is a system exhibiting two CDW transitions that can be identified from anomalies in the temperature-dependent resistance. In the context of the Peierls' mechanism, these anomalies stem from partial gapping of the Fermi surface, which removes conduction electrons. Nonlinear transport is observed in the vicinity of the transitions, ²² a hallmark of CDW systems, but the Kohn anomaly is not seen in the phonon spectrum near the CDW wavevectors. ²³ The nature of the pseudogaps in the Fermi surface corresponding to its CDW transitions has been measured in photoemission ^{24,25} and reflectivity studies, ²⁶ but the situation is still uncertain and the classification of NbSe₃ is a subject of ongoing research. Very recent studies have demonstrated the importance of electron–electron interactions and self-organization of electrons, leading to effectively 1D behavior. ^{27–29}

For type I CDWs, the relevant materials have bandstuctures that are highly one-dimensional. This requirement is fulfilled by several linear-chain compounds, such as the TMTs, the molybdenum bronzes, and some 1D organic salts. ^{30,31} The structure of the linear-chain compounds is that of weakly coupled molecular chains. Electron conduction is highly anisotropic and preferential along the chains. ³² Consistent with Peierls' picture, the lattice reconstruction is accompanied by a metal-insulator transition. In some cases, the Fermi surface is completely gapped, but in most real materials with complex Fermi surfaces, only partial gapping occurs and the metal-insulator transition manifests itself as a resistive anomaly.

For type II CDWs, the Fermi surface is quasi-2D or higher in dimensionality. While there is no appreciable structure in $\chi(\mathbf{q},\omega)$ to indicate FSN, there is considerable softening of the phonon spectrum. In this case, one should search for strong coupling to excitations elsewhere in the system. Importantly, these materials need not exhibit a

TABLE I. Summary of important characteristics of materials discussed in the text. Emphasized in bold are the group IV transition metal trichalcogenides, which are the focus of this article.

Compound	Class	Crystal symmetry	Chain complexity ^a	Global metallicity ^b
Niobium triselenide (NbSe ₃)	TMTs	Triclinic	NbSe ₃ -type	Metallic
Tantalum trisulfide (TaS ₃)	TMTs	Monoclinic/orthorhombic	TaS ₃ -type	Metallic
Zirconium tritelluride (ZrTe ₃)	TMTs	Monoclinic	ZrSe ₃ -type	Metallic
Hafnium tritelluride (HfTe ₃)	TMTs	Monoclinic	ZrSe ₃ -type	Metallic
Titanium tritelluride (TiTe ₃)	TMTs	Monoclinic	ZrSe ₃ -type	Metallic
Titanium trisulfide (TiS ₃)	TMTs	Monoclinic	ZrSe ₃ -type	Semiconducting
Niobium diselenide (NbSe ₂)	TMDs	Hexagonal		Metallic
Tantalum disulfide (TaS ₂)	TMDs	Hexagonal		Metallic
Tantalum diselenide (TaSe ₂)	TMDs	Hexagonal		Metallic
Titanium diselenide (TiSe ₂)	TMDs	Hexagonal	•••	Semiconducting

^aZrSe₃-type, TaS₃-type, and NbSe₃-type correspond to 1, 2, and 3 inequivalent chains per unit cell, respectively.

^bConsidering bulk material. Global refers to behavior away from typical CDW-resistive anomalies.

metal-insulator transition. Candidates include several of the transition metal dichalcogenides (TMDs) such as NbSe2, TaSe2, and TaS2.3 NbSe₂ exhibits both superconductivity and a structural transition associated with a CDW,34 but with a wavevector unrelated to Fermi surface nesting^{18,35} and no metal-insulator transition.³⁶ TaSe₂ and TaS₂ exhibit particularly rich CDW dynamics, in which transitions from different CDW states occur based on temperature and pressure.³³ TaS₂, for example, transitions from a commensurate to nearly commensurate, and to incommensurate CDW state with increasing temperature in a wide range from 100 to 600 K.38 The emergence in the past decade of novel techniques for the handling of ultrathin vander-Waals materials has provided new opportunities for the investigation of CDW phenomena in the TMDs. The propensity of these materials to exfoliate in the form of thin crystalline sheets provides an opportunity to manipulate their collective electronic states, through quantum confinement to quasi-two-dimensional layers and by electrostatic gating of their carriers. Thus, a great body of work has emerged on the subject of the tunability of the CDW states in nanoscale TMD devices and heterostructures.

Type III CDWs occur in the regime where electron–electron correlations are important, a property that is neglected in the above discussions of the type I and II materials. A common method to estimate if such interactions are important is to define an interaction parameter (r_s) , which accounts for the relative contributions of the Coulomb energy (E_C) and Fermi energy (E_F) to the total energy. ^{52–54} One can express r_s as a ratio of the average interparticle distance (a) to the effective Bohr radius (a_B) , ⁵²

$$r_s = \frac{E_C}{E_F} = \frac{a}{a_B}. (2)$$

Since a is inversely proportional to the carrier concentration (albeit with weaker dependence in higher dimensions), it is concluded that the relative strength of electron-electron interactions is greater for more dilute systems. There are many possible ground states for a system in which electron-electron interactions dominate, some of which are suggested to involve a CDW. Two examples are Overhauser's exchange-instability waves, 55-59 associated with a spin or charge density wave having wavevector $\mathbf{q} = 2\mathbf{k}_{\mathrm{F}}$, and Wigner's electronic crystal, associated with a CDW with $\mathbf{q} = 4\mathbf{k}_{\mathrm{F}}$. Examples Examples type III CDWs include those found in the cuprates and manganites, which are known for their complex and varied phases associated with charge ordering.⁶³ It is important to note that the charge ordering in a CDW would consist of delocalized electrons while conventional charge ordering consists of localized electrons. The applicability of arguments related to CDW formation in explaining the phenomena exhibited by these materials is an intensely debated topic extending back more than a decade. 64-71 Noise spectroscopy measurements seem to confirm that CDW physics are relevant in some capacity in piecing together the picture of transport in at least the manganites.

It should be emphasized that in many CDW systems $r_s \gg 1$, suggesting the importance of electron–electron interactions in determining the nature of the collective state. ⁵⁴ In the low-temperature commensurate CDW phase of TaS₂, the system is insulating and strongly influenced by electron–electron interactions. ^{38,78} Depending on the details of heating and cooling, one can observe behavior consistent with a band insulator or a Mott–Hubbard insulating state. ⁷⁹ Within the insulating state, one can also realize so-called "hidden

CDW states" on ultrafast timescales. 46,80 One of the very few semiconducting systems to exhibit a CDW and associated structural transition is the narrow bandgap semiconductor TiSe₂. It has been suggested that the CDW formation is electronically driven and that TiSe₂ forms an excitonic insulator, 81–84 but the origin of the CDW is still controversial. The except time-resolved studies suggest that excitonic pairing due to hybridization of the conduction and valence bands states initializes the CDW while electron–phonon coupling is necessary to maintain it. Separately, the existence of superconductivity and its competition with the CDW state has been investigated by pressure, electrostatic doping, and intercalation, shedding light on the mechanisms behind the formation of these collective states. Separately in the room-temperature nearly commensurate CDW phase. The dynamics of a narrow bandgap also determine the characteristics of TaS₂ in its room-temperature nearly commensurate CDW phase.

II. COLLECTIVE STATES IN THE GROUP IV TMTs

An instructive way to classify TMTs is in terms of the complexity of their linear chains. The prototypical CDW materials TaS3 and NbSe₃ crystallize with two and three inequivalent chains per unit cell, respectively. The complexity of the resulting Fermi surface is reflected by the degree of interchain coupling and crystal symmetry. As an example, NbSe3 exhibits triclinic structure, the lowest threedimensional symmetry class, and exhibits several CDWs that are isotropic and whose transition temperatures are intimately tied to the degree of interchain coupling. The quasi-one-dimensional structure of the group IV TMTs makes them well suited to explorations of the different CDW models described above. The materials that we will discuss all crystallize in the ZrSe3-type structure, which is a lowsymmetry monoclinic class with space group P21/m. Materials with this structure have only one type of chain per unit cell. TMTs are comprised of transition metal (M) and chalcogen (X) atoms in the stoichiometric form MX₃. The crystal structure is comprised of trigonal prisms (formed from X_2^{2-} and X^{2-} anions flanking a M^{4+} cation) which stack along the b-axis, forming a chain-like structure. These chains are linked along the a direction by interprism M-X bonds, forming a layer that tessellates the ab-plane. The planes are connected along the c-axis by weak van der Waals (vdW) forces [Fig. 1(a)]. The net result is a quasi-1D structure characterized by anisotropic electronic and optical properties.

The recent interest in the studies of CDW phenomena in TMT materials has been enabled by the availability of synthetic techniques for high-quality TMT crystals and their suitability for mechanical exfoliation and device fabrication. Large TMT crystals can be conveniently grown via a direct reaction between elemental precursors, 99 as illustrated in Fig. 1(b). This shows TiS3 crystals several centimeters long, in which individual quasi-1D chains can be visualized by transmission electron microscopy [Fig. 1(c)].⁷⁶ Theoretical calculations reveal that the TiS3 cleavage energies are lower than the cleavage energy for graphene layers in graphite crystals, suggesting the ease of exfoliation of TMT materials.⁷⁶ Furthermore, the calculated energies required for breaking weak vdW interactions between the 2D layers, and between quasi-1D chains within the layers, are comparable. Consequently, exfoliation of TMT crystals often results in them splitting along the crystallographic b direction, yielding narrow nanoribbons with very smooth, straight edges. Figure 1(d) shows a representative atomic force microscopy image of uniform, mechanically exfoliated TiS₃ nanoribbons on Si/SiO₂ with thickness ranging

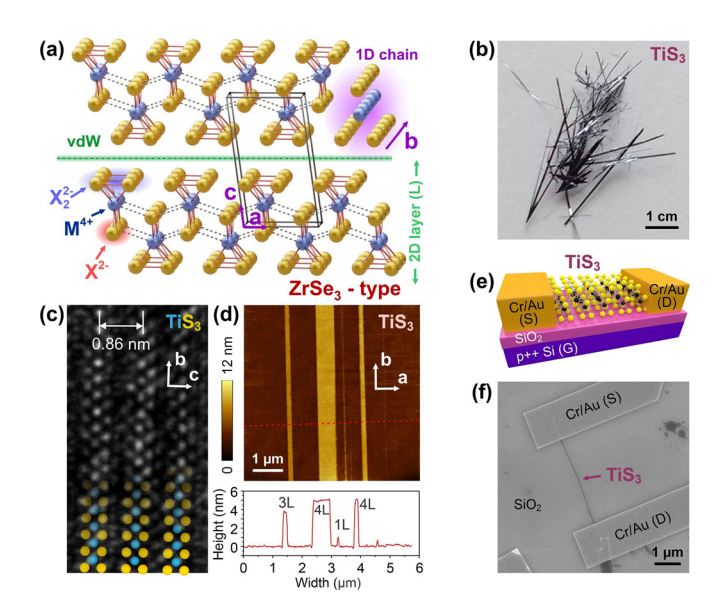


FIG. 1. (a) One of the simplest structures formed by the TMTs is the ZrSe₃-type structure with one type of MX₃ chain. ⁷³ More complex materials crystallize with two (TaSe₃-type) or three (NbSe₃-type) inequivalent chains. ^{74,75} (b) Optical photograph of TiS₃ crystals grown by a direct reaction between metallic titanium and sulfur vapor in a sealed ampule at 550 °C. ⁷⁶ (c) TEM image of quasi-1D chains in a TiS₃ crystal. ⁷⁶ Ti, blue spheres; S, yellow spheres. (d) AFM image of mechanically exfoliated TiS₃ nanoribbons on Si/SiO₂ (top), and their height profiles showing thicknesses ranging from 1 to 4 layers (L) (bottom). ⁷⁶ Reprinted with permission from Lipatov *et al.*, ACS Nano **12**(12), 12713–12720 (2018). Copyright 2018 American Chemical Society. (e) and (f) Scheme and SEM image of a representative two-terminal device based on a mechanically exfoliated TiS₃ nanoribbon. ⁷⁷ Reprinted with permission from Lipatov *et al.*, Nanoscale **7**(29), 12291–12296 (2015). Copyright 2015 by a CC-BY 3.0 license.

from 1 to 4 layers. Such nanoribbons can be conveniently used for the fabrication of electronic devices $^{76,77,101-105}$ [Figs. 1(e) and 1(f)] that provide testbeds for the investigation of transport phenomena in TMTs.

The metallic members of the group IV TMTs have been extensively studied due to the coexistence of superconductivity and CDW ordering. The interplay of which can be manipulated by temperature, pressure, and doping (chemical or electrostatic). The remaining group IV TMTs are semiconducting, yet experimental results indicate members such as TiS₃ exhibit behavior consistent with CDW formation. These methods reflect a general approach to studying phase changes and rich collective state physics in a variety of other material systems such as the TMDs. ¹⁰⁶

A. ZrTe₃

Several decades after its initial synthesis, characterization, ⁹⁸ and classification, ¹⁰⁰ it was discovered experimentally that ZrTe₃ is semi-metallic ^{107,108} and exhibits both CDW and superconducting transitions. ^{109–111} Both phenomena are related to Fermi surface instabilities and thus the interplay of their electronic states make this material a testbed for particularly interesting physics. The origin of its different

phases can be understood in terms of the topology of the multifaceted Fermi surface of $ZrTe_3$ [Fig. 2(a)]. This surface comprises an admixture of quasi-1D sheets, a 3D sheet, and a van Hove singularity at the intersection of such topologies. ^{112,113} The CDW transition occurs due to nesting of the quasi-1D sheets, as well as strong electron–phonon coupling while the superconducting transition is associated with electronic states on the 3D and intersecting surfaces. ¹¹²

The CDW transition of ZrTe₃ occurs at a critical temperature of $T_{CDW} \approx 63 \text{ K}$ and is associated with a commensurate ordering vector which connects the quasi-1D sheets of the Fermi surface. Determination of this vector by both band structure calculations 112,113 and electron diffraction measurements 114 results in good agreement. Additionally, diffuse x-ray scattering experiments reveal a strong Kohn anomaly in the phonon spectrum as the temperature is lowered in the vicinity of T_{CDW} [Fig. 2(b)]. However, the mean-field theory of CDWs^{10,11} predicts a particular temperature dependence of the Kohn anomaly that is not obeyed in experiment. This is an indication of the importance of higher-dimensional fluctuations in determining the nature of the CDW transition in real materials. This is a wellunderstood problem and corrections to the mean-field theory exist in the literature. 12,13 With the advent of more precise spectroscopy methods (e.g., ARPES), fluctuations and their implications can be more readily studied. Raman spectroscopy studies have illustrated the importance of electron-phonon interactions in determining the quantitative properties of the CDW transition. 97,115 Several of the Ramanactive phonon modes of ZrTe3 show broadening and asymmetry consistent with coupling to the CDW state [Fig. 2(c)]. Finally, a recent ARPES study revealed an anomaly in the quasiparticle scattering rate across the 3D portion of the Fermi surface at T_{CDW} , suggesting an interaction between the CDW and superconducting states.1

From electrical measurements, 109,110 evidence of CDW formation is given by an anomaly that appears in the temperature dependence of the resistance at T_{CDW} . Since \mathbf{q}_{CDW} only has components in \mathbf{c} and \mathbf{a} , this anomaly is not observed along the \mathbf{b} direction. In a type I picture (FSN driven), such resistive anomalies are caused by destruction of the quasi-1D components of the Fermi surface as T_{CDW} is approached. Accompanying this change, carriers are driven into the CDW state and, thus, the resistance is modified. In the 1D Peierls picture, the Fermi surface is completely destroyed, leading to a metal-insulator transition, but in $ZrTe_3$ the metallicity is maintained by the other components of its Fermi surface that are unaffected by the transition. This idea has been confirmed by detailed ARPES measurements which show the evolution of the relevant Fermi surface components with temperature.

The superconducting transition of ZrTe₃ occurs at a critical temperature of $T_c \approx 2$ K along the **a** direction and $T_c \approx 5$ K along the **b** direction. Furthermore, the transition along **a** is sharp while it is significantly more gradual in the **b** direction. Flat, 111,119 Thus, early investigations described the superconductivity as filamentary in nature. 111 In contrast, the more familiar bulk superconductivity is isotropic. 120 Later studies of the specific heat uncovered a humplike anomaly below T_c and a strong deviation from the expected functional form $(C_p/T=\gamma+\beta T)$, where γ and β are the electronic and lattice specific heat coefficients, respectively. This is a typical characteristic of a bulk superconductor. The authors presented a model in which there is a crossover from filamentary to bulk superconductivity with decreasing temperature, so-called "mixed bulk-filament superconductivity." 1119

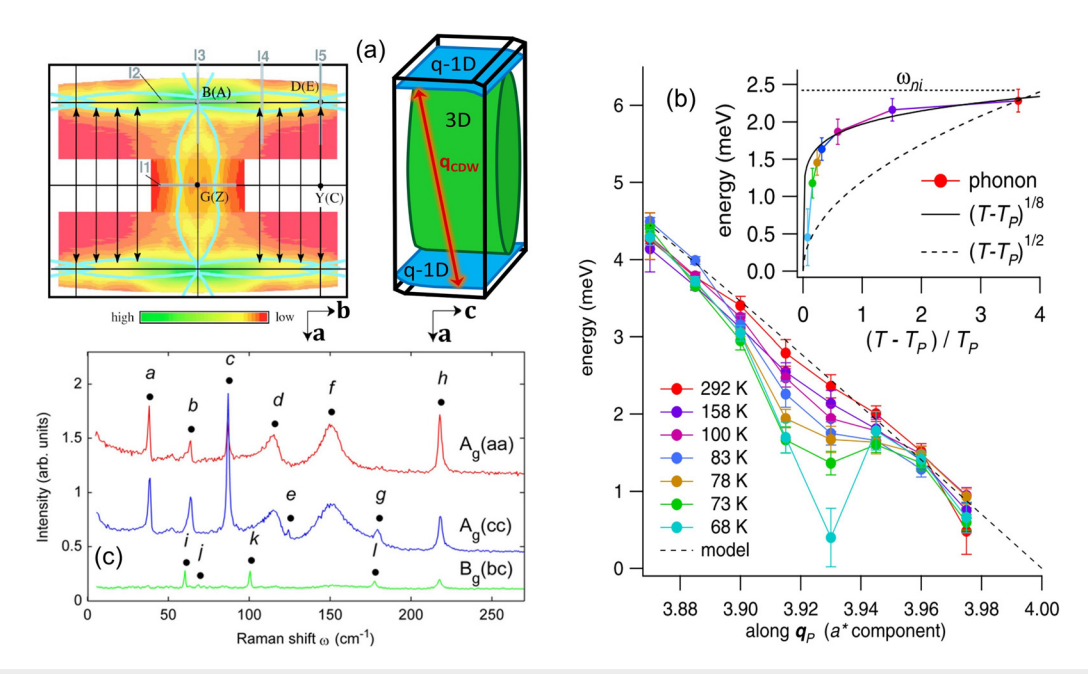


FIG. 2. (a) The Fermi surface of ZrTe $_3$ measured by ARPES indicates a broad 3D component in the vicinity of the G-point that is flanked on either side by quasi-1D sheets that comprise the Brillouin zone boundaries. The van Hove singularity linking the two topologies occurs at the B-point where they intersect. ARPES data reprinted with permission from Yokoya *et al.*, Phys. Rev. B **71**(14), 140504 (2005). Copyright 2005 American Physical Society. (b) The Kohn anomaly is observed near the component of ${\bf q}_{\rm CDW}$ (${\bf q}_{\rm p} \approx 3.93$) as temperature is lowered below the transition temperature. Reprinted with permission from Hoesch *et al.*, Phys. Rev. Lett. **102**(8), 086402 (2009). Copyright 2009 American Physical Society. (c) Several vibrational modes in the Raman spectrum deviate from the expected Lorenzian line shape, reflecting their coupling to the CDW state. Reprinted with permission from Hu *et al.*, Phys. Rev. B **91**(14), 144502 (2015). Copyright 2015 American Physical Society.

this model, the high-temperature filamentary state is characterized by short-range, attractive interactions between local electron pairs which behave as bosons. At low temperature, long-range order develops and conventional Cooper pairs give rise to the observed bulk superconductivity. It is concluded that this unique situation is due to the nature of the intersecting region of the Fermi surface, ¹¹⁹ a point suggested in earlier theoretical calculations. ¹¹² Recent experimental results in which the effects of pressure and magnetic field were taken into account support the picture of local-pair formation. ¹²¹

The pressure dependence of both the CDW and superconducting state of ZrTe3 has been investigated, largely for the purpose of exploring their interplay. 118,122,123 The essential behavior is captured in the phase diagram of Fig. 3(b). As the pressure is initially increased, T_{CDW} increases while T_c vanishes near ≈ 0.5 GPa. With further increase in pressure, however, CDW formation is suppressed above ≈ 5 GPa, and the superconductivity reemerges. This reentrant superconductivity can be explained in terms of Fermi surface dynamics. In a simple picture, the CDW dynamics are confined to the quasi-1D sheets on the Fermi surface while the superconducting dynamics are confined to the remnant portions. If pressure changes the shape of the Fermi surface, the remnant surface after the CDW transition will be modulated, thus affecting the density of states available to participate in the superconducting transition. 118 One can estimate the change in density of states near the Fermi level due to the CDW transition directly from the temperature dependence of resistance 124,125 and such an analysis qualitatively supports this scenario. 118 In a recent study, pressures of up to 36 GPa were applied to $ZrTe_3$ samples and T_c was observed to be as high as 7.1 K at 28 GPa.

The dynamics of the CDW and superconductivity can also be modulated by chemical doping. To this end, various compounds of $ZrTe_3$ have been created by either intercalation $^{127-129}$ (Ni_x $ZrTe_3$, Cu_x ZrTe₃, and Ag_x ZrTe₃) or substitution (ZrTe_{3-x} Se_x). In the intercalated compound $Ni_{0.05}ZrTe_3$, T_{CDW} was suppressed from its nominal value of 60 K to 41 K. Simultaneously, T_c was enhanced from 2 K to 3.1 K. 127 Similarly, in $Cu_{0.05}ZrTe_3$ T_{CDW} was suppressed slightly while T_c was enhanced to 3.8 K. 128 In both cases, the adatoms weakly perturb the lattice parameters, but change the properties of the Fermi surface such that the coexistence of the CDW and superconducting states is suppressed, leaving only superconductivity favored. Several authors have investigated the substitutional compound ZrTe_{3-x} Se_x to understand the quenching of the CDW state due to increasing substitutional disorder. The phase diagram of Fig. 3(a) illustrates how with increasing Se content, the CDW state disappears in favor of superconductivity.¹ Optical reflectivity and ARPES measurements indicate that with increasing Se content, the CDW order becomes more short-ranged as the lattice becomes structurally disordered.¹³

B. HfTe₃

In spite of the fact that they are isostructural⁹⁹ and predicted to have both similar electronic properties and sensitivity to external pressure, ¹¹² HfTe₃ has been studied far less than ZrTe₃. It should be noted that HfTe₃ is difficult to synthesize, requiring tight growth conditions. Additionally, it is not stable in air, quickly transforming from its native metallic state to an insulating one in a matter of hours.¹³⁴ Despite these difficulties, several authors have managed to create devices to

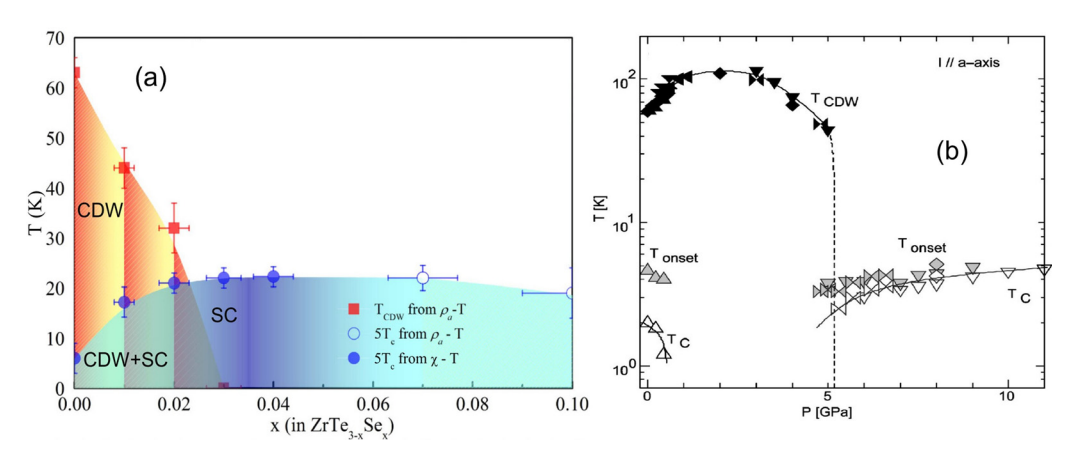


FIG. 3. (a) Phase diagram of ZrTe₃ doped with small amounts of Se. ¹¹⁷ Adapted with permission from Zhu *et al.*, Sci. Rep. **6**, 26974 (2016). Copyright 2016 Author(s), licensed under a Creative Commons Attribution 4.0 license. (b) Pressure-dependent phase diagram of ZrTe₃ revealing the interplay of CDW and superconducting states and reentrant superconductivity. ¹¹⁸ Reprinted with permission from Yomo *et al.*, Phys. Rev. B **71**(13), 132508 (2005). Copyright 2005 by the American Physical Society.

confirm the existence of CDW and superconducting states. An initial study reported on the strain induced dynamics of HfTe₃ thin films grown on a Hf substrate. The lattice mismatch between the layers induced local wrinkles in the HfTe₃ thin film that could be investigated

by several microscopy and spectroscopy methods. A scanning-tunneling microscopy (STM) topographic image of a wrinkle is shown in Fig. 4(a), with corresponding line scans along and across it [Fig. 4(b)]. The differential conductance is measured by the probe [Fig. 4(c)] and reflects

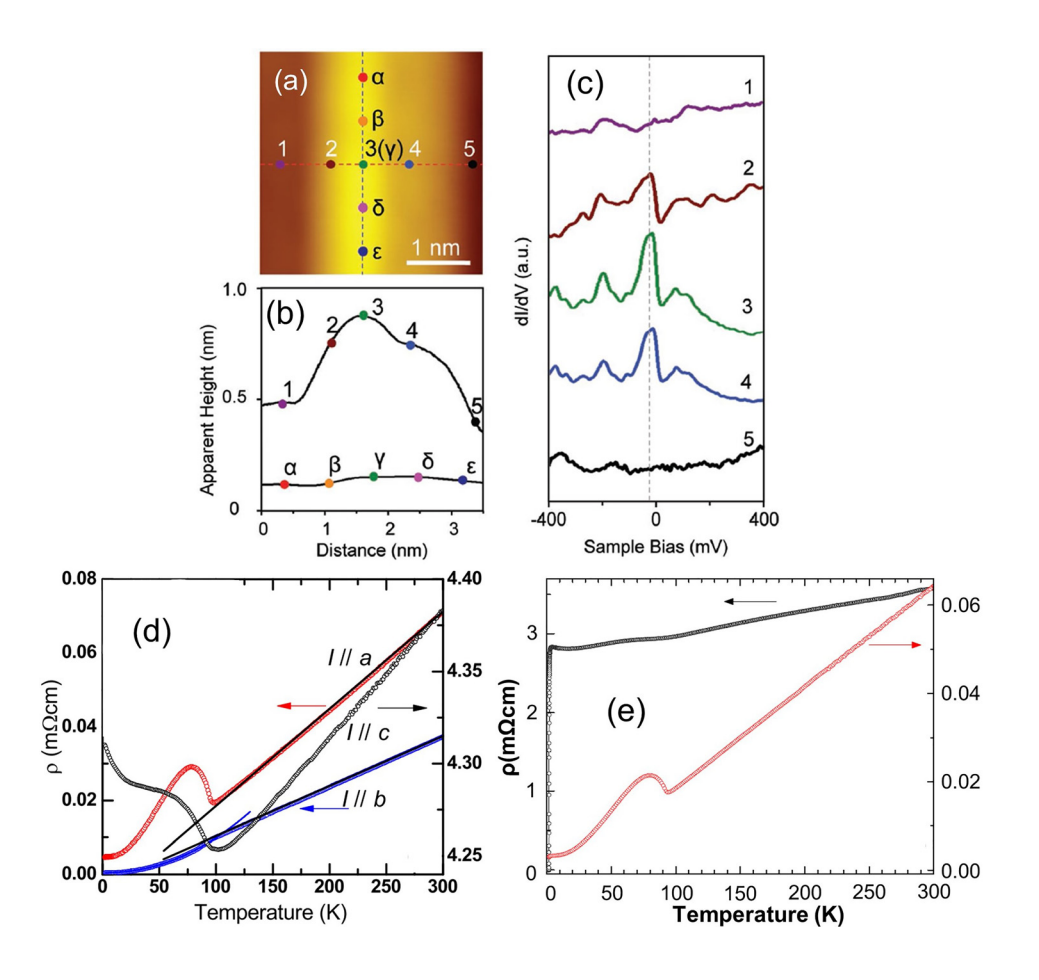


FIG. 4. (a)-(c) Scanning-tunneling microscopy (STM) and scanning-tunneling spectroscopy (STS) measurements of wrinkles formed on a HfTe₃/Hf heterostructure which exhibit large modulations in the local density of states. 132 Reprinted with permission from Wang et al., Adv. Electron. Mater. **2**(12), 1600324 (2016). Copyright 2016 John Wiley and Sons. (d) Highly anisotropic temperature-dependent resistance of HfTe₃ samples. Comparison of the temperature of the te temperaturedependent resistance for polycrystalline (left axis) and crystalline (right axis) samples. 133 Adapted with permission from Li et al., Phys. Rev. B 96(17), 174510 (2017). Copyright 2017 American Physical Society.

changes in the local density of states. The conclusion is that new electronic states are localized near the wrinkles which may be used for nanoelectronic devices such as waveguides. 132 In a more complex heterostructure (HfTe₃/HfTe₅/Hf), the superconducting spectrum of the HfTe₃ was measured by scanning-tunneling spectroscopy (STS). The film was found to have a relatively low $T_c \approx 1.2 \, \mathrm{K}^{135}$ Shortly after, the CDW and superconducting states were observed together in more traditional current-voltage measurements on polycrystalline HfTe₃ samples. The usual resistive anomaly was observed at $T_{CDW} \approx 82 \text{ K}$ and superconductivity emerged at $T_c \approx 1.8$ K. Under application of modest pressure (1 GPa), T_{CDW} was found to shift to higher temperatures in a similar way to ZrTe₃. ¹³⁴ The nature of the various phases of HfTe₃ was made clearer by a systematic study of both polycrystalline and crystalline samples. 133 The polycrystalline samples exhibited both the CDW transition ($T_{CDW} \approx 80 \text{ K}$) and superconductivity ($T_c \approx 2 \text{ K}$), while the crystalline one showed only a CDW transition (at a slightly increased temperature of \approx 93 K). The absence of superconductivity in the crystalline sample suggests the importance of disorder to mediating the superconducting transition. Additionally, the authors concluded from magnetic susceptibility and specific heat measurements that the superconductivity is filamentary in nature. Electrical measurements along the different crystallographic directions exhibit significant differences [Fig. 4(d)]. In contrast to ZrTe₃, where the CDW forms in the ac plane, the CDW transition is prominent along the a axis, but has a weaker effect on conduction along the b direction. This suggests that the CDW forms in the ab plane. The behavior along the c axis is very different, 133 exhibiting a metal-insulator transition near T_{CDW} . Finally, HfTe₃ films in the few-chain limit were recently synthesized inside multiwall carbon nanotubes. In the limit of three or fewer chains, the HfTe3 underwent a metal-semiconductor transition due to a structural change of the chains from trigonal prismatic to triginal antiprismatic.1

C. TiTe₃

Synthesis of TiTe₃ has only recently been demonstrated, under challenging conditions of confined growth in multiwall carbon nanotubes, and the resulting material has only been shown to be stable in the few-chain limit.¹³⁷ There are a few references to this material in the literature, with the earliest study stating that it could not be synthesized despite a wide attempted parameter space.³⁸ In a theoretical study, it was determined that the cleavage energy of this material is larger than that of many of the triselenides and trisulfides, making it more difficult to exfoliate. TiTe₃ is predicted to be metallic with a large density of states near the Fermi energy, suggesting the possibility of realizing superconductivity.¹³⁸ This would be consistent with what is observed in the other TMT members that we have discussed. Density-functional theory (DFT) calculations in the recent growth study indicated that TiTe₃ in the one-chain limit is semiconducting with a 0.680 eV bandgap.¹³⁷

D. TiS₃

Titanium trisulfide (TiS₃) is a van der Waals material⁷⁶ that has been studied in several different contexts. The aspect that has gained the most attention in recent studies involves its anisotropic optoelectronic and thermoelectric properties. The electrical properties of TiS₃ are also of significant interest and display this anisotropy as well as several indications of collective state formation, believed to be

related to a CDW. These behaviors are typically found in metallic materials, so it is particularly interesting to see them in a compound that is semiconducting for a large range of temperature. It should be emphasized that investigating the field-effect is much more tenable in nanoscale and semiconducting CDW materials than in their metallic counterparts. The ability to vary carrier concentration via the field-effect 77,102 is imperative for probing the nature of collective state formation as shown in earlier studies on NbSe, and TaS. 150,151

mation as shown in earlier studies on NbSe₃ and TaS₃. 150,151 Some of the earliest studies of TiS₃ determined $^{152-155}$ that it was an n-type band semiconductor with a metal-insulator transition (MIT) near $T_{MIT} \approx 220$ K. X-ray diffraction studies were unable to detect distortion of the crystal in the vicinity of T_{MIT} and it was determined that the transition is not associated with a CDW. 152 Below T_{MIT} , the conductivity exhibited a strong frequency dependence and the thermopower decreased markedly below 100 K. These observations were used to explain the importance of disorder and localization in transport.¹⁵⁴ The MIT has been observed in several subsequent studies on the bulk material 139,140,142,156-158 and, more recently, in nanowires, 104,141,159 in which its onset temperature can be controlled by variation of the carrier density via the field-effect [Fig. 5(a)]. 104 Several different mechanisms have been suggested to account for the occurrence of the MIT. The first of these is a Peierls distortion, which structural measurements seem to discount at present. ¹⁵² The second is a competition between the decreasing carrier concentration and increasing mobility as temperature is decreased. This interpretation stems from observed differences between the Hall and field-effect mobilities, behavior which is attributed to the influence of CDW fluctuations on the field-effect. The net result is that the field-effect mobility is lower than the Hall mobility. In essence, it is suggested that there is no true MIT and that TiS3 remains semiconducting up to at least room-temperature. 160 The third interpretation comes from a transport model in which TiS3 becomes a degenerate semiconductor above T_{MIT} . In a separate study on h-BN encapsulated TiS₃ devices, both the Hall and field-effect mobilities were found to exhibit powerlaw dependencies on temperature ($\mu \propto T^{\gamma}$), with γ consistent with phonon-limited scattering mechanisms. The difference between the power-law fits and magnitude of the different mobilities was explained in terms of the Hall scattering coefficient.¹⁵⁹ Interestingly, the fieldeffect mobility was found to be larger than the Hall mobility while their maxima occurred in the same temperature range. This is in contrast to other studies where the Hall mobility was larger and had its maximum at lower temperature than the field-effect mobility.¹³⁹ It is expected that a comprehensive model considering phonon scattering mechanisms at high temperatures and CDW dynamics at lower temperatures is required to accurately describe the observed mobility trend in TiS_3 .

TiS₃ is isostructural to the materials discussed thus far, but has a markedly lower room-temperature carrier concentration 153 (around $10^{18}~\rm cm^{-3}$) than the typical metallic TMTs such as NbSe₃, TaS₃, ZrTe₃, or HfTe₃. Despite this, several characteristics of its electrical transport, observed in many experiments, suggest collective state formation. In thick samples, three cusp singularities are observed in the temperature-dependent resistance at $T_1=23~\rm K,\ T_2=53~\rm K,\ and$ $T_3=103~\rm K$ [Fig. 5(d)]. 141,142 In the mean-field CDW theory, cusplike singularities are predicted for a second-order transition to the CDW ground state with long-range 3D order. 11 In nanoscale samples, resistive anomalies are also observed, but the results are somewhat

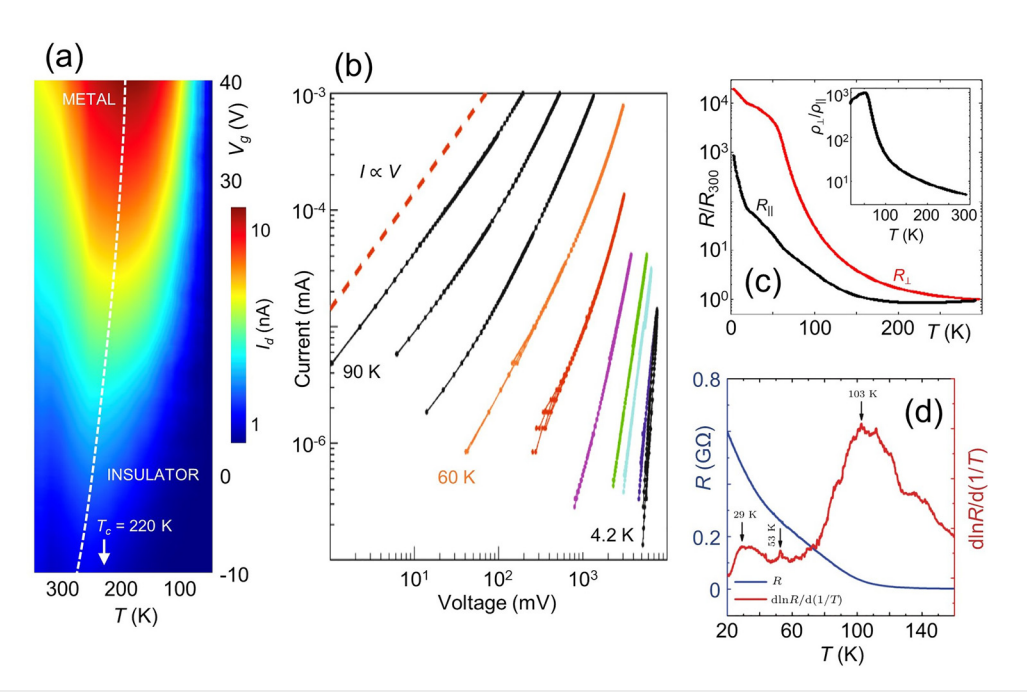


FIG. 5. (a) The MIT in TiS₃ nanowires can be influenced by the channel carrier concentration, which increases with increasing gate voltage on the vertical axis. 104 Adapted with permission from [Randle *et al.*, ACS Nano **13**(1), 803–811 (2019). Copyright 2019 American Chemical Society. (b) Power-law nonlinearity is observed in the current-voltage characteristic of bulk TiS₃ samples at temperatures below 60 K. 139 Adapted with permission from Gorlova *et al.*, Physica B **460**, 11–15 (2015). Copyright 2015 Elsevier. (c) Bulk TiS₃ exhibits modest resistance anisotropy at room-temperature, but it is greatly enhanced at low temperatures. 140 Reprinted with permission from Gorlova *et al.*, Physica B **407**, 1707–1710 (2012). Copyright 2012 Elsevier. (d) Thick TiS₃ samples have three resistive anomalies in the temperature-dependent resistance. Their exact positions vary slightly between samples, but in a 50 nm sample, they are observed at $T_1 = 23$ K, $T_2 = 53$ K, and $T_3 = 103$ K. 141 Adapted with permission from Huang *et al.*, Chin. Phys. B **26**(6), 067302 (2017). Copyright 2017 IOP Publishing. Very similar values are observed in truly bulk samples.

inconsistent. In a study 141 performed on a nanowire 15-nm thick, presumed transitions associated with T_2 and T_3 were evident at lowered temperatures of 46 K and 85 K, while no evidence was found of the expected transition at T_1 . In another report, ¹⁵⁹ in contrast, performed on a nanosheet 26-nm thick, the features expected at T_1 and T_2 were observed at 20 K and 50 K, respectively, while structure indicative of T_3 was now absent. In both studies, it was moreover found that these temperature scales could be modified by varying the carrier concentration in the device via the field-effect. The common feature of these experiments, that the anomalies observed in the nanoscale devices all occur at temperatures below those of the bulk material, can be attributed to finite-size effects. 162 These are well established in the more widely studied CDW materials such as TaS₃¹⁶³ and NbSe₃. ¹⁶⁴ In short, as the dimensions of the sample shrink, the tendency for T_{CDW} to decrease, and for the CDW transition to broaden, 162 as the sample size is reduced is consistent with the influence of CDW fluctuations in the mean-field theory. 11,1

Power-law behavior has been observed in the current-voltage characteristic of bulk TiS₃ samples at the lowest voltages measured below T_2 . This behavior is seen along all crystallographic directions with the highest nonlinearity observed along the **c** direction [Fig. 5(b)]. ¹⁵⁷ In most metallic CDW materials, this nonlinearity manifests itself as a fairly well-defined threshold in the conductance. Below this threshold, the conductance is small and constant, indicating an Ohmic, single-particle contribution. At larger voltages, the conductance rises nonlinearly as the CDW becomes unpinned and freely

carries current in the channel. 166 Often, however, the situation is not as simple and various secondary effects such as CDW phase slip or thermal creep can cause the observed power-law behavior with no clear threshold. Such effects are most prominently manifested in finite-size samples. 162 In an experiment performed on TiS₃ nanoribbons, for example, it was found that anomalies in the power-law dependence of the current were correlated with the different CDW transition temperatures. 141 For a system with several CDWs such as NbSe₃, the threshold voltage for the onset of nonlinear conduction is known to have extrema at the various transition temperatures.²² The correlation reported in TiS₃ nanoribbons¹⁴¹ is therefore perhaps reasonable.²² Exceptionally strong nonlinearity over a large voltage range is observed in nanowires and is found to be carrier concentration dependent. The nonlinearity is greatest at the lowest carrier concentrations, creating a situation where the differential conductance is quenched for small voltages. 104 Non-Ohmic behavior at low fields can manifest from contact resistance, a problem exacerbated in lowdimensional materials, 167,168 but such effects have been shown experimentally ¹⁰⁴ and theoretically ^{169,170} to be negligible in TiS₃ with standard contact metals. It should be noted that at low-temperature, saturation of the differential resistance has been observed for very low fields in an h-BN encapsulated TiS₃ nanoribbon, ¹⁵⁹ an observation more typical of CDW systems.

Reflecting the anisotropic structure of TiS₃, the temperature-dependent resistance measured along different crystallographic axes is found to be inequivalent. All of the resistive anomalies (T_1, T_2, T_3) are

observed in both of the in-plane directions [(a) and (b)]. T_3 , however, is not observed in the van der Waals c direction which separates layers. ¹⁵⁷ Because there are multiple transition temperatures and they display anisotropy, it has been suggested that two CDWs may form in TiS₃, along and across the chains. ¹⁵⁷ This claim is consistent with an earlier XRD study that revealed additional reflections forming along the a direction. ¹⁴⁰ Aside from these features, the resistivity anisotropy is measured to be $\rho_c: \rho_a: \rho_b \approx 20: 5: 1$ at room-temperature. The anisotropy increases significantly below 100 K and near T_2 it is $\rho_c: \rho_a: \rho_b \approx 10^6: 10^3: 1$ [Fig. 5(c)]. ¹⁵⁷ The significance of T_2 is moreover established by the behavior of the magnetoresistance below this temperature, which indicates charge or magnetic ordering. ¹⁵⁸

Frequency-dependent noise and metastable states are wellestablished phenomena that are intrinsic to CDW systems. 166 One characteristic not often discussed in the context of CDWs, however, is mesoscopic conductance fluctuations. In the context of normal metals, one can observe, for example, universal conductance fluctuations in wires 171-173 and Aharonov-Bohm oscillations in rings. 174,175 Usually, these phenomena arise from interference in the single-electron wavefunction. The electron phase coherence required to observe the fluctuations is only preserved at low temperatures (≈ 1 K) and is washed out quickly with increasing temperature. 176-181 The situation is quite different for CDW systems, in which the phase coherence lengths can be several tens of micrometers long at cryogenic temperatures and there are large fluctuations of the order parameter. Conductance fluctuations have been measured in rings of TaS₃¹⁶⁵ and through columnar defects in NbSe₃. ¹⁸² In TaS₃ rings, Aharonov–Bohm oscillations were observed [Fig. 6(a)] and they persisted to high temperature. 165 The magneto-conductance oscillations arise from coupling of the CDW to a vector potential generated by the magnetic field. 183 Recently, mesoscopic conductance fluctuations have been observed in TiS3 nanowires [Figs. 6(b) and 6(c)]. Their temperature dependence is nonmonotonic, having a global maximum near one of the CDW transition temperatures $(T_2 \approx 40 \text{ K})$. Moreover, the fluctuations persist to temperatures exceeding 200 K, suggestive of a large coherence length in the system. Both of these observations strongly suggest that the fluctuations are related to the dynamics of CDW formation and decoherence with increasing temperature.

Overall, the experimental results in bulk and nanoscale TiS₃ samples are consistent with those expected of a CDW material. Moreover, the semiconducting nature of TiS3 suggests the formation of an unconventional CDW in this material that is likely more related to charge ordering and electron-electron interactions (type III) than electron-phonon interactions (type I and II). The mounting experimental evidence in favor of CDW formation must be corroborated by measurements that can probe crystal and electronic structure to verify this assertion, and distinguish the CDW state from other possible ground states. A collection of methods traditionally employed to characterize CDW materials are summarized in Table II. As stated earlier, XRD studies of TiS₃¹⁴⁰ have revealed additional lattice reflections at low temperature, suggesting an incipient structural change, but further study is required. Specifically, those methods which can probe the coupling of electronic degrees of freedom to the lattice, such as Raman spectroscopy, and the different scanning probe methods would be important for characterizing a system displaying type III behavior. Aside from the long coherence lengths suggested by mesoscopic conductance fluctuations in transport measurements, 104 there is no direct

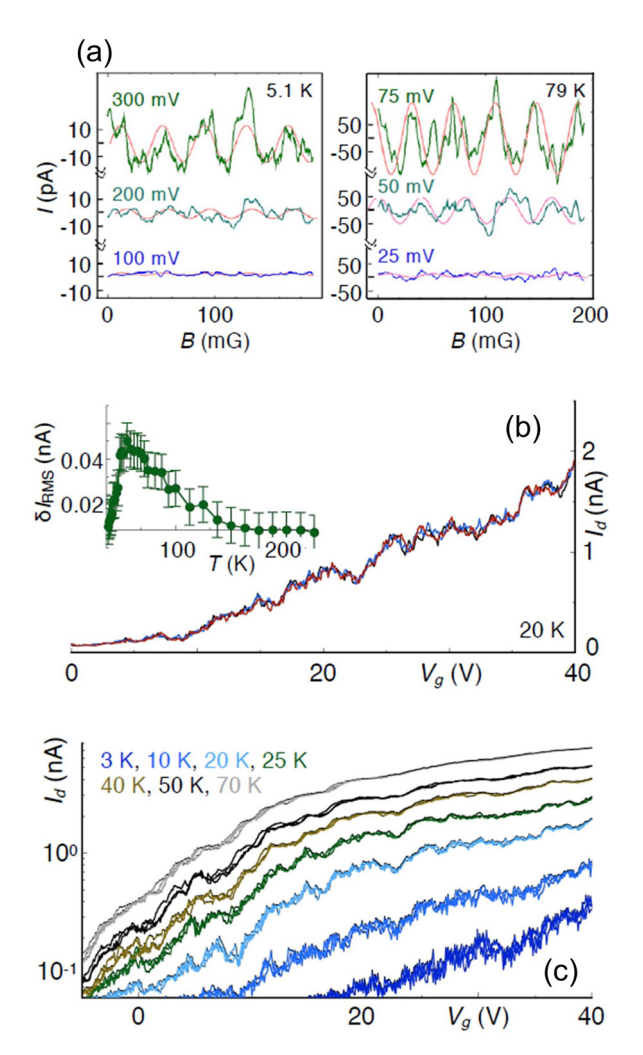


FIG. 6. (a) Robust Aharonov–Bohm oscillations are observed in TaS₃ at high temperatures (5.1 K and 79 K) due to the large coherence length of the CDW in this material. Adapted with permission from Tsubota *et al.*, Europhys. Lett. **97**, 57011 (2012). Copyright 2012 IOP Publishing. (b) and (c) Mesoscopic conductance fluctuations are observed in TiS₃ nanowires as a function of carrier density. They persist to high temperature due to the existence of a CDW with large phase coherence length. Adapted with permission from Randle *et al.*, ACS Nano **13**(1), 803–811 (2019). Copyright 2019 American Chemical Society.

evidence of CDW domain formation or coherence in TiS₃, which could be explored by STM, STS, or AFM studies (Table II). We note that Raman studies have been performed on TiS₃, 76,184 but not at low enough temperatures or with the intention of probing collective state physics.

As a final note, we consider a recent first-principles DFT study¹⁸⁵ of TiS₃ monolayers in which a type I CDW with its origin in the Peierls distortion is revealed for large electronic densities such that the Fermi level is within the conduction band (i.e., under conditions where the Fermi surface exists). Depending on the carrier concentration, TiS₃ was predicted to exhibit different electrical properties. In the doping interval 0–0.1 electrons per unit cell, it was found that the Fermi

TABLE II. Summary of experimental techniques commonly implemented for characterization of the crystal and electronic structure of CDW materials.

Technique name ^a	Structure probed	Scope	Information extracted ^{b,c}
X-ray diffraction	Crystal	Macroscopic	Crystal structure and symmetry, lattice constants/angles, structural phase transitions
Diffuse x-ray scattering	Crystal	Macroscopic	Sharp scattering peak near $\mathbf{q}_{\mathbf{CDW}}$ reflections gives information about pinning/defects
Inelastic x-ray scattering	Crystal	Macroscopic	X-ray energy loss from different phonon branches can reveal the Kohn anomaly, thus identifying q _{CDW}
Inelastic neutron scattering	Crystal	Macroscopic	Neutron energy loss from different phonon branches can reveal the Kohn anomaly, thus identifying q _{CDW}
Photoemission spectroscopy	Electronic	Microscopic	Bandstructure mapping/occupation, Fermi surface topology, and direct imaging of CDW gap/pseudogap
Reflectance spectroscopy	Electronic	Macroscopic	Redistribution of spectral weight provides information about Fermi surface gapping and CDW fluctuations
Scanning tunneling spectroscopy	Electronic	Microscopic	Determination of the local density of states (LDOS) helps to map CDW coherence lengths and pinning mechanisms
Raman spectroscopy	Crystal and electronic	Macroscopic	Light scattering reveals CDW related vibrational modes, el- ph coupling quantified by linewidth changes and peak shifting
Selected area electron diffraction	Crystal and electronic	Microscopic	Superlattice imaging gives components of ${\bf q}_{\rm CDW}$ and can also give information about CDW commensurability
Scanning tunneling microscopy	Crystal and electronic	Microscopic	Local density of states (LDOS) measurement. Reveals CDW domains, periodicity, commensurability, and pinning
Atomic force microscopy	Crystal and electronic	Microscopic	Surface electronic charge density measurement. Reveals CDW domains, periodicity, commensurability, and pinning

^aTemperature, time, and angle-resolved versions of many of these experimental techniques are available.

surface is closed and corresponds to a 2D metal. For 0.18-0.3 electrons per unit cell, the Fermi surface opens, revealing a quasi-1D nature and the possibility, dependent upon the exact doping level, of nesting. Many of these observations stem from the fact that interchain coupling in TiS₃ is nontrivial. ¹⁸⁵ Two studies considering the electric field-effect in TiS₃ discovered that the resistive anomaly near 50 K (T_2) experiences a shift and narrows with increasing carrier concentration. ^{159,186} It has been suggested that this narrowing is consistent with the high density Peierls distortion considered in the DFT study. ¹⁸⁵ This CDW is predicted to form in an effectively metallic state of TiS₃ and is derived from the mono and few layer bandstructures. At this time, we suggest that this type I CDW be considered separately from the type III one discussed above.

III. CONCLUSION

The conventional wisdom that the Peierls distortion alone gives rise to the CDW state has been challenged by recent simulations and experiments on prototypical CDW materials with complex structures such as NbSe₃, which have several inequivalent chains in their unit cell and thus complex bandstructures. The group IV TMTs are a class of materials recently considered for CDW physics that are structurally simpler, having only one inequivalent chain per unit cell. The metallic tritellurides ZrTe₃ and HfTe₃ exhibit both CDW and superconducting transitions, with rich interplay that can be explored by various pressure dependent and doping experiments. ZrTe₃ is fairly well studied,

while HfTe3 and the recently synthesized TiTe3 require further inquiry. The results from the literature suggest that these materials exhibit CDW physics closer to that envisioned by Peierls (type I) but also underline the importance of more general electron-phonon interactions in stabilizing the state (type II). We, however, tentatively suggest that these materials are type I, in that the Fermi surface nesting mechanism drives the CDW while other contributions are secondary. Regardless of origin, these materials are promising for continued exploration into how different collective states interact and development of nanoelectronic devices based on this interaction. TiS3 is a group IV TMT that is semiconducting but exhibits behavior that can be attributed to collective state formation and, most likely, to CDWs. Most discussion of CDWs is confined to metallic materials, so further investigation into this material is called for. Collective states forming in compounds in the semiconducting state are thought to be related to electron-electron interactions instead of Fermi surface dynamics. Some examples include Wigner crystallization, formation of an excitonic insulator (such as in TiSe2), or Mott dielectrization (such as in TaS₂). These possibilities have been also suggested for some time by other authors. 142 TiS₃ can then be said to exhibit a type III CDW, driven by charge ordering. Measurements that continue to reveal the true nature of prototypical CDW materials like NbSe3 are necessary to determine the nature of the collective state and presumed CDW in TiS₃. Scanning probe methods, in particular, can be used to discern structures formed by correlated electrons in detail, including the local

^bThis is not intended to be comprehensive, but rather focuses on information relevant to characterizing a CDW.

 $^{^{\}circ}$ Temperature-dependent experiments with these methods will also reveal information about the CDW ordering temperature(s) (T_{CDW}).

order of a Wigner crystal. 187 The exploration of the unconventional CDW in semiconducting compounds such as TiS_3 presents the opportunity for development of novel electronic devices that combine the aspects of CDW conductors and band semiconductors.

ACKNOWLEDGMENTS

Work at Buffalo was supported by the U.S. Department of Energy, Office of Basic Energy Sciences, Division of Materials Sciences and Engineering (No. DE-FG02-04ER46180), the National Science Foundation (No. NSF-ECCS 1740136), and nCORE, a wholly owned subsidiary of the Semiconductor Research Corporation (SRC), through the Center on Antiferromagnetic Magneto-electric Memory and Logic (Task Nos. 2760.001 and 2760.002).

DATA AVAILABILITY

Data sharing is not applicable to this article as no new data were created or analyzed in this study.

REFERENCES

- ¹R. E. Peierls, *The Quantum Theory of Solids* (Oxford University Press, Oxford, UK, 1955).
- ²H. Fröhlich, Proc. R. Soc. A **223**, 296–305 (1954).
- ³H. Fukuyama, J. Phys. Soc. Jpn. **41**, 513–541 (1976).
- ⁴H. Fukuyama and P. A. Lee, Phys. Rev. B 17, 535–541 (1978).
- ⁵P. A. Lee and H. Fukuyama, Phys. Rev. B **17**, 542–548 (1978).
- ⁶P. A. Lee and T. M. Rice, Phys. Rev. B **19**, 3970–3980 (1979).
- ⁷D. S. Fisher, Phys. Rev. Lett. **50**, 1486–1489 (1983).
- ⁸D. S. Fisher, Phys. Rev. B **31**, 1396–1427 (1985).
- ⁹O. Narayan and D. S. Fisher, Phys. Rev. Lett. **68**, 3615–3618 (1992).
- ¹⁰M. J. Rice and S. Strässler, Solid State Commun. **13**, 125–128 (1973).
- ¹¹G. Grüner, Density Waves in Solids (CRC Press, Florida, USA, 1994).
- ¹²P. A. Lee, T. M. Rice, and P. W. Anderson, Phys. Rev. Lett. **31**, 462–465 (1973)
- ¹³M. J. Rice and S. Strässler, Solid State Commun. **13**, 1389–1392 (1973).
- ¹⁴L. Yue, S. Xue, J. Li, W. Hu, A. Barbour, F. Zheng, L. Wang, J. Feng, S. B. Wilkins, C. Mazzoli, R. Comin, and Y. Li, Nat. Commun. 11, 98 (2020).
- ¹⁵P. Monceau, J. Richard, and M. Renard, Phys. Rev. B **25**, 931–947 (1982).
- ¹⁶S. Ravy, S. Rouziére, J. P. Pouget, S. Brazovskii, J. Marcus, J. F. Bérar, and E. Elkaim, Phys. Rev. B 74, 174102 (2006).
- ¹⁷S. Brazovskii, C. Brun, Z.-Z. Wang, and P. Monceau, Phys. Rev. Lett. **108**, 096801 (2012).
- ¹⁸M. D. Johannas and I. I. Mazin, *Phys. Rev. B* 77, 165135 (2008).
- ¹⁹X. Zhu, Y. Cao, J. Zhang, E. W. Plummer, and J. Guo, Proc. Natl. Acad. Sci. U. S. A. 112, 2367–2371 (2015).
- ²⁰X. Zhu, J. Guo, J. Zhang, and E. W. Plummer, Adv. Phys.-X 2, 622–640 (2017).
- ²¹W. Kohn, Phys. Rev. Lett. 2, 393–394 (1959).
- ²²R. M. Flemming, Phys. Rev. B 22, 5606–5612 (1980).
- ²³H. Requardt, J. E. Lorenzo, P. Monceau, R. Currat, and M. Krisch, Phys. Rev. B 66, 214303 (2002).
- ²⁴J. Schäfer, E. Rotenberg, S. D. Kevan, P. Blaha, R. Claessen, and R. E. Thorne, Phys. Rev. Lett. **87**, 196403 (2001).
- ²⁵J. Schäfer, M. Sing, R. Claessen, E. Rotenberg, X. J. Zhou, R. E. Thorne, and S. D. Kevan, Phys. Rev. Lett. **91**, 066401 (2003).
- ²⁶A. Perucchi, L. Degiorgi, and R. E. Thorne, Phys. Rev. B 69, 195114 (2004).
- ²⁷C. W. Nicholson, C. Berthod, M. Puppin, H. Berger, M. Wolf, M. Hoesch, and C. Monney, Phys. Rev. Lett. 118, 206401 (2017).
- ²⁸M. A. Valbuena, P. Chudzinski, S. Pons, S. Conejeros, P. Alemany, E. Canadell, H. Berger, E. Frantzeskakis, J. Avila, M. C. Asensio, T. Giamarchi, and M. Grioni, Phys. Rev. B 99, 075118 (2019).

- ²⁹C. W. Nicholson, E. F. Schwier, K. Shimada, H. Berger, M. Hoesch, C. Berthod, and C. Monney, Phys. Rev. B 101, 045412 (2020).
- **30**P. Monceau, Adv. Phys. **61**, 325–581 (2012).
- ³¹Low-Dimensional Electronic Properties of Molybdenum Bronzes and Oxides, edited by C. Schlenker (Kluwer Academic Publishers, AA Dordrecht, The Netherlands, 1989).
- 32R. E. Thorne, Phys. Today 49(5), 42-47 (1996).
- ³³J. A. Wilson, F. J. D. Salvo, and S. Mahajan, Adv. Phys. 24, 117–201 (1975).
- ³⁴M. M. Ugeda, A. J. Bradley, Y. Zhang, S. Onishi, Y. Chen, W. Ruan, C. Ojeda-Aristizabal, H. Ryu, M. T. Edmonds, H.-Z. Tsai, A. Riss, S.-K. Mo, D. Lee, A. Zettl, Z. Hussain, Z.-X. Shen, and M. F. Crommie, Nat. Phys. 12, 92–97 (2016).
- 35 M. Calandra, I. I. Mazin, and F. Mauri, Phys. Rev. B 80(R), 241108 (2009).
- ³⁶M. Naito and S. Tanaka, J. Phys. Soc. Jpn. **51**, 219–227 (1982).
- ³⁷J. A. Wilson, F. J. D. Salvo, and S. Mahajan, Phys. Rev. Lett. 32, 882–885 (1974).
- ³⁸B. Sipos, A. F. Kusmartseva, A. Akrap, H. Berger, L. Forró, and E. Tutiš, Nat. Mater. 7, 960–965 (2008).
- ³⁹M. Yoshida, Y. Zhang, J. Ye, R. Suzuki, Y. Imai, S. Kimura, A. Fujiwara, and Y. Iwasa, Sci. Rep. 4, 7302 (2014).
- 40 Y. Yu, F. Yang, X. F. Lu, Y. J. Yan, Y.-H. Cho, L. Ma, X. Niu, S. Kim, Y.-W. Son, D. Feng, S. Li, S.-W. Cheong, X. H. Chen, and Y. Zhang, Nat. Nanotechnol. 10, 270–276 (2015).
- ⁴¹M. J. Hollander, Y. Liu, W.-J. Lu, L.-J. Li, Y.-P. Sun, J. A. Robinson, and S. Datta, Nano Lett. 15, 1861–1866 (2015).
- ⁴²G. Liu, B. Debnath, T. R. Pope, T. T. Salguero, R. K. Lake, and A. A. Balandin, Nat. Nanotechnol. 11, 845–850 (2016).
- ⁴³Y. Ishiguro, K. Bogdanov, N. Kodama, M. Ogiba, T. Ohno, A. Baranov, and K. Takai, J. Phys. Chem. C 124, 27176–27184 (2020).
- ⁴⁴Q. Stahl, M. Kusch, F. Heinsch, G. Garbarino, N. Kretzschmar, K. Hanff, K. Rossnagel, J. Geck, and T. Ritschel, Nat. Commun. 11, 1247 (2020).
- ⁴⁵C. Zhu, Y. Chen, F. Liu, S. Zheng, X. Li, A. Chaturvedi, J. Zhou, Q. Fu, Y. He, Q. Zeng, H. J. Fan, H. Zhang, W.-J. Liu, T. Yu, and Z. Liu, ACS Nano 12, 11203–11210 (2018).
- 46W. Wen, C. Dang, and L. Xie, Chin. Phys. B 28, 058504 (2019).
- 47W. Wen, Y. Zhu, C. Dang, W. Chen, and L. Xie, Nano Lett. 19, 1805–1813 (2019).
- ⁴⁸M. Mahajan, K. Murali, N. Kawatra, and K. Majumdar, Phys. Rev. Appl. 11, 024031 (2019).
- ⁴⁹R. Salgado, A. Mohammadzadeh, F. Kargar, A. Geremew, C.-Y. Huang, M. A. Bloodgood, S. Rumyantsev, T. T. Salguero, and A. A. Balandin, Appl. Phys. Express 12, 037001 (2019).
- ⁵⁰ A. G. Khitun, A. K. Geremew, and A. A. Balandin, IEEE Electron Device Lett. 39, 1449–1452 (2018).
- ⁵¹W. Li and G. V. Naik, Opt. Mater. Express **9**, 497–503 (2019).
- 528. Kravchenko, Strongly Correlated Electrons in Two Dimensions (Pan Stanford Publishing, Danvers, MA, 2017).
- 53V. M. Pudalov, Sov. Phys. Usp. 34, 542–544 (1991).
- ⁵⁴M. M. Fogler, S. Teber, and B. I. Shklovskii, Phys. Rev. B 69, 035413–035411–18 (2004).
- ⁵⁵A. W. Overhauser, Phys. Rev. Lett. **4**, 462–465 (1960).
- ⁵⁶A. W. Overhauser, J. Phys. Chem. Solids **13**, 71–80 (1960).
- ⁵⁷A. W. Overhauser, Phys. Rev. **128**, 1437–1452 (1962).
- ⁵⁸A. W. Overhauser, Phys. Rev. **167**, 691–698 (1968).
- ⁵⁹ A. W. Overhauser, Phys. Rev. B **3**, 3173–3182 (1971).
- 60 E. Wigner, Phys. Rev. 46, 1002-1011 (1934).
- 61 E. Wigner, Trans. Faraday Soc. 34, 678–685 (1938).
- 62H. J. Schulz, Phys. Rev. Lett. 71, 1864–1867 (1993).
- 63C.-W. Chen, J. Choe, and E. Morosan, Rep. Prog. Phys. 79, 084505 (2016).
- ⁶⁴S. Cox, J. Singleton, R. D. McDonald, A. Migliori, and P. B. Littlewood, Nat. Mater. 7, 25–30 (2008).
- ⁶⁵B. Fisher, J. Genossar, L. Patlagan, S. Kar-Narayan, X. Moya, J. C. Loudon, and N. D. Mathur, Nat. Mater. 9, 688 (2010).
- ⁶⁶S. Cox, J. Singleton, R. D. McDonald, A. Migliori, and P. B. Littlewood, Nat. Mater. 9, 689 (2010).
- ⁶⁷B. Fisher, J. Genossar, L. Patlagan, and G. M. Reisner, J. Magn. Magn. Mater. 322, 1239–1242 (2010).

- ⁶⁸Y. M. Wang, B. H. Ge, Y. X. Cui, R. C. Yu, S. Chen, and Z. F. Ren, Mater. Today Phys. 5, 7–11 (2018).
- 69 B. Fisher, J. Genossar, L. Patlagan, S. Kar-Narayan, X. Moya, D. Sánchez, P. A. Midgley, and N. D. Mathur, J. Phys.: Condens. Matter 22, 275602 (2010).
- ⁷⁰R. Schmidt, Phys. Rev. B 77, 205101 (2008).
- ⁷¹M. Smari, R. Hamdi, J. Prado-Gonjal, R. Cortés-Gil, E. Dhahri, F. Mompean, M. García-Hernández, and R. Schmidt, Phys. Chem. Chem. Phys. 22, 11625–11636 (2020).
- 72C. Barone and S. Pagnao, Coatings 11, 96 (2021).
- ⁷³J. Gopalakrishnan and K. S. Nanjundaswamy, Bull. Mater. Sci. 5, 287–306 (1983).
- 74S. K. Srivastava and B. N. Avasthi, J. Mater. Sci. 27, 3693–3705 (1992).
- ⁷⁵J. A. Wilson, Phys. Rev. B **19**, 6456–6468 (1979).
- ⁷⁶A. Lipatov, M. J. Loes, H. Lu, J. Dai, P. Patoka, N. S. Vorobeva, D. S. Muratov, G. Ulrich, B. Kästner, A. Hoehl, G. Ulm, X. C. Zeng, E. Rühl, A. Gruverman, P. A. Dowben, and A. Sinitskii, ACS Nano 12, 12713–12720 (2018).
- ⁷⁷ A. Lipatov, P. M. Wilson, M. Shekhirev, J. D. Teeter, R. Netusila, and A. Sinitskii, Nanoscale 7, 12291–12296 (2015).
- ⁷⁸H. Lin, W. Huang, K. Zhao, S. Qiao, Z. Liu, J. Wu, X. Chen, and S.-H. Ji, Nano Res. 13, 133–137 (2020).
- 79Y. D. Wang, W. L. Yao, Z. M. Xin, T. T. Han, Z. G. Wang, L. Chen, C. Cai, Y. Li, and Y. Zhang, Nat. Commun. 11, 4215 (2020).
- ⁸⁰D. Cho, G. Gye, J. Lee, S.-H. Lee, L. Wang, S.-W. Cheong, and H. W. Yeom, Nat. Commun. 8, 392 (2017).
- 81 H. Cercellier, C. Monney, F. Clerc, C. Battaglia, L. Despont, M. G. Garnier, H. Beck, P. Aebi, L. Patthey, H. Berger, and L. Forró, Phys. Rev. Lett. 99, 146403 (2007)
- 82 C. Monney, E. F. Schwier, M. G. Garnier, N. Mariotti, C. Didiot, H. Beck, P. Aebi, H. Cercellier, J. Marcus, C. Battaglia, H. Berger, and A. N. Titov, Phys. Rev. B 81, 155104 (2010).
- 83C. Monney, C. Battaglia, H. Cercellier, P. Aebi, and H. Beck, Phys. Rev. Lett. 106, 106404 (2011).
- ⁸⁴M. Cazzaniga, H. Cercellier, M. Holzmann, C. Monney, P. Aebi, G. Onida, and V. Olevano, Phys. Rev. B 85, 195111 (2012).
- 85 K. Rossnagel, J. Phys.: Condens. Matter 23, 213001 (2011).
- ⁸⁶M. D. Watson, O. J. Clark, F. Mazzola, I. Marković, V. Sunko, T. K. Kim, K. Rossnagel, and P. D. C. King, Phys. Rev. Lett. 122, 076404 (2019).
- 87C. Lian, S.-J. Zhang, S.-Q. Hu, M.-X. Guan, and S. Meng, Nat. Commun. 11, 43 (2020)
- 88 E. Morosan, H. W. Zandbergen, B. S. Dennis, J. W. G. Bos, Y. Onose, T. Klimczuk, A. P. Ramirez, N. P. Ong, and R. J. Cava, Nat. Phys. 2, 544–550 (2006)
- 89 A. F. Kusmartseva, B. Sipos, H. Berger, L. Forró, and E. Tutiš, Phys. Rev. Lett. 103, 236401 (2009).
- 90 L. J. Li, E. C. T. O'Farrell, K. P. Loh, G. Eda, B. Özyilmaz, and A. H. C. Neto, Nature 529, 185–189 (2016).
- ⁹¹S. Yan, D. Iaia, E. Morosan, E. Fradkin, P. Abbamonte, and V. Madhavan, Phys. Rev. Lett. 118, 106405 (2017).
- ⁹²A. Kogar, G. A. de la Pena, S. Lee, Y. Fang, S. X.-L. Sun, D. B. Lioi, G. Karapetrov, K. D. Finkelstein, J. P. C. Ruff, P. Abbamonte, and S. Rosenkranz, Phys. Rev. Lett. 118, 027002 (2017).
- ⁹³Q. Hu, S. Xu, X. Guo, H. Liu, Z. Chen, B. Wang, and R. Ang, J. Phys.: Condens. Matter 32, 425602 (2020).
- ⁹⁴M. Bovet, S. van Smaalen, H. Berger, R. Gaal, L. Forró, L. Schlapbach, and P. Aebi, Phys. Rev. B 67, 125105 (2003).
- 95T. Yokoya, T. Kiss, A. Chainani, S. Shin, and K. Yamaya, Phys. Rev. B 71, 140504 (2005).
- ⁹⁶M. Hoesch, A. Bosak, D. Chernyshov, H. Berger, and M. Krisch, Phys. Rev. Lett. **102**, 086402 (2009).
- 97 Y. Hu, F. Zheng, X. Ren, J. Feng, and Y. Li, Phys. Rev. B 91, 144502 (2015).
- 98 F. K. McTaggart and A. D. Wadsley, Aust. J. Chem. 11, 445–457 (1958).
- 99L. Brattas and A. Kjekshus, Acta Chem. Scand. 26, 3441–3449 (1972).
- 100 S. Furuseth, L. Brattås, and A. Kjekshus, Acta Chem. Scand. 29a, 623–631 (1975).
- 101 J. O. Island, M. Buscema, M. Barawi, J. M. Clamagirand, J. R. Ares, C. Sánchez, I. J. Ferrer, H. S. J. van der Zant, G. A. Steele, and A. Castellanos-Gomez, Adv. Opt. Mater. 2, 641–645 (2014).

- 102 J. O. Island, M. Barawi, R. Biele, A. Almazán, J. M. Clamagirand, J. R. Ares, C. Sánchez, H. S. J. van der Zant, J. V. Álvarez, R. D'Agosta, I. J. Ferrer, and A. Castellanos-Gomez, Adv. Mater. 27, 2595–2601 (2015).
- 103 A. J. Molina-Mendoza, J. O. Island, W. S. Paz, J. M. C, J. R. Ares, E. Flores, F. Leardini, C. Sánchez, N. Agraït, G. Rubio-Bollinger, H. S. J. van der Zant, I. J. Ferrer, J. J. Palacios, and A. Castellanos-Gomez, Adv. Funct. Mater. 27, 1605647 (2017).
- 104M. Randle, A. Lipatov, A. Kumar, C.-P. Kwan, J. Nathawat, B. Barut, S. Yin, K. He, N. Arabchigavkani, R. Dixit, T. Komesu, J. Avila, M. C. Asensio, P. A. Dowben, A. Sinitskii, U. Singisetti, and J. P. Bird, ACS Nano 13, 803–811 (2019)
- 105 D. S. Muratov, V. O. Vanyushin, N. S. Vorobeva, P. Jukova, A. Lipatov, E. A. Kolesnikov, D. Karpenkov, D. V. Kuznetsov, and A. Sinitskii, J. Alloys Compd. 815, 152316 (2020).
- ¹⁰⁶Z. Wang, R. Li, C. Su, and K. P. Loh, SmartMat 1, e1013 (2020).
- 107 T. J. Wieting, A. Grisel, and F. Lévy, Physica B 105, 366–369 (1981).
- 108 S. C. Bayliss and W. Y. Liang, J. Phys. C 14, L803 (1981).
- 109 S. Takahashi, T. Sambongi, and S. Okada, J. Phys. Colloques 44, C3-1733-1736 (1983).
- ¹¹⁰S. Takahashi, T. Sambongi, J. W. Brill, and W. Roark, Solid State Commun. 49, 1031–1033 (1984).
- ¹¹¹H. Nakajima, K. Nomura, and T. Sambongi, Physica B **143**, 240–243 (1986).
- ¹¹²C. Felser, E. W. Finckh, H. Kleinke, F. Rocker, and W. Tremel, J. Mater. Chem. 8, 1787–1798 (1998).
- 113 K. Stöwe and F. R. Wagner, J. Solid State Chem. 138, 160–168 (1998).
- ¹¹⁴D. J. Eaglesham, J. W. Steeds, and J. A. Wilson, J. Phys. C **17**, L697 (1984).
- ¹¹⁵S. L. Gleason, Y. Gim, T. Byrum, A. Kogar, P. Abbamonte, E. Fradkin, G. J. MacDougall, D. J. V. Harlingen, X. Zhu, C. Petrovic, and S. L. Cooper, Phys. Rev. B 91, 155124 (2015).
- ¹¹⁶S.-P. Lyu, L. Yu, J.-W. Huang, C.-T. Lin, Q. Gao, J. Liu, G.-D. Liu, L. Zhao, J. Yuan, C.-T. Chen, Z.-Y. Xu, and X.-J. Zhou, Chin. Phys. B 27, 087503 (2018)
- 117 X. Zhu, W. Ning, L. Li, L. Ling, R. Zhang, J. Zhang, K. Wang, Y. Liu, L. Pi, Y. Ma, H. Du, M. Tian, Y. Sun, C. Petrovic, and Y. Zhang, Sci. Rep. 6, 26974 (2016).
- ¹¹⁸R. Yomo, K. Yamaya, M. Abliz, M. Hedo, and Y. Uwatoko, Phys. Rev. B 71, 132508 (2005).
- ¹¹⁹K. Yamaya, S. Takayanagi, and S. Tanda, Phys. Rev. B **85**, 184513 (2012).
- 120 J. Bardeen, L. N. Cooper, and J. R. Schrieffer, Phys. Rev. 108, 1175–1204 (1957).
- ¹²¹S. Tsuchiya, K. Matsubayashi, K. Yamaya, S. Takayanagi, S. Tanda, and Y. Uwatoko, New J. Phys. 19, 063004 (2017).
- 122K. Yamaya, M. Yoneda, S. Yasuzuka, Y. Okajima, and S. Tanda, J. Phys.: Condens. Matter 14, 10767–10770 (2002).
- ¹²³K. Igarashi, S. Yasuzuka, K. Inagaki, S. Tanda, Y. Okajima, M. Hedo, Y. Uwatoko, and K. Yamaya, J. Phys. IV France 12, 97–98 (2002).
- 124 K. Kawabata, J. Phys. Soc. Jpn. 54, 762–770 (1985).
- ¹²⁵M. Ido, Y. Okayama, T. Ijiri, and Y. Okajima, J. Phys. Soc. Jpn. 59, 1341–1347 (1990).
- ¹²⁶K. Gu, R. A. Susilo, F. Ke, W. Deng, Y. Wang, L. Zhang, H. Xiao, and B. Chen, J. Phys.: Condens. Matter 30, 385701 (2018).
- ¹²⁷H. Lei, X. Zhu, and C. Petrovic, Europhys. Lett. **95**, 17011 (2011).
- ¹²⁸X. Zhu, H. Lei, and C. Petrovic, Phys. Rev. Lett. **106**, 246404 (2011).
- 129 C. S. Yadav and P. L. Paulose, J. Phys.: Condens. Matter 24, 235702 (2012).
- ¹³⁰M. Chinotti, J. Ethiraj, C. Mirri, X. Zhu, L. Li, C. Petrovic, and L. Degiorgi, Phys. Rev. B 97, 045117 (2018).
- ¹³¹M. Hoesch, L. Gannon, K. Shimada, B. J. Parrett, M. D. Watson, T. K. Kim, X. Zhu, and C. Petrovic, Phys. Rev. Lett. 122, 017601 (2019).
- 132 Y.-Q. Wang, X. Wu, Y.-F. Ge, Y.-L. Wang, H. Guo, Y. Shao, T. Lei, C. Liu, J.-O. Wang, S.-Y. Zhu, Z.-L. Liu, W. Guo, K. Ibrahim, Y.-G. Yao, and H.-J. Gao, Adv. Electron. Mater. 2, 1600324 (2016).
- ¹³³J. Li, J. Peng, S. Zhang, and G. Chen, Phys. Rev. B **96**, 174510 (2017).
- 134 S. J. Denholme, A. Yukawa, K. Tsumura, M. Nagao, R. Tamura, S. Watauchi, I. Tanaka, H. Takayanagi, and N. Miyakawa, Sci. Rep. 7, 45217 (2017).
- 135Y.-Q. Wang, X. Wu, Y.-L. Wang, Y. Shao, T. Lei, J.-O. Wang, S.-Y. Zhu, H. Guo, L.-X. Zhao, G.-F. Chen, S. Nie, H.-M. Weng, K. Ibrahim, X. Dai, Z. Fang, and H.-J. Gao, Adv. Mater. 28, 5013–5017 (2016).

- 136S. Meyer, T. Pham, S. Oh, P. Ercius, C. Kisielowski, M. L. Cohen, and A. Zettl, Phys. Rev. B 100, 041403 (2019).
- ¹³⁷S. Stonemeyer, J. D. Cain, S. Oh, A. Azizi, M. Elasha, M. Thiel, C. Song, P. Ercius, M. L. Cohen, and A. Zettl, J. Am. Chem. Soc. 143, 4563–4568 (2021).
- ¹³⁸Y. Jin, X. Lia, and J. Yang, Phys. Chem. Chem. Phys. **17**, 18665–18669 (2015).
- ¹³⁹I. G. Gorlova, S. G. Zybtsev, V. Y. Pokrovskii, N. B. Bolotina, S. Y. Gavrilkin, and A. Y. Tsvetkov, Physica B 460, 11–15 (2015).
- ¹⁴⁰I. G. Gorlova, S. G. Zybtsev, V. Y. Pokrovskii, N. B. Bolotina, I. A. Verin, and A. N. Titov, Physica B 407, 1707–1710 (2012).
- ¹⁴¹C. Huang, E. Zhang, X. Yuan, W. Wang, Y. Liu, C. Zhang, J. Ling, S. Liu, and F. Xiu, Chin. Phys. B 26, 067302 (2017).
- ¹⁴²I. G. Gorlova and V. Y. Pokrovskii, JETP Lett. **90**, 295–298 (2009).
- ¹⁴³M. Li, J. Dai, and X. C. Zeng, Nanoscale 7, 15385–15391 (2015).
- 144J. O. Island, R. Biele, M. Barawi, J. M. Clamagirand, J. R. Ares, C. Sánchez, H. S. van der Zant, I. J. Ferrer, R. D'Agosta, and A. Castellanos-Gomez, Sci. Rep. 6, 22214 (2016).
- ¹⁴⁵J. Dai, M. Li, and X. C. Zeng, WIREs Comput. Mol. Sci. 6, 211–222 (2016).
- ¹⁴⁶J. O. Island, A. J. Molina-Mendoza, M. Barawi, R. Biele, E. Flores, J. M. Clamagirand, J. R. Ares, C. Sánchez, H. S. J. van der Zant, and R. D'Agosta, 2D Mater. 4, 022003 (2017).
- ¹⁴⁷A. Patra and C. S. Rout, RSC Adv. **10**, 36413–36438 (2020).
- 148N. Tripathi, V. Pavelyev, P. Sharma, S. Kumar, A. Rymzhina, and P. Mishra, Mater. Sci. Semicond. Process. 127, 105699 (2021).
- 149H. Yi, T. Komesu, S. Gilbert, G. Hao, A. J. Yost, A. Lipatov, A. Sinitskii, J. Avila, C. Chen, M. C. Asensio, and P. A. Dowben, Appl. Phys. Lett. 112, 052102 (2018).
- 150 T. L. Adelman, S. V. Zaitsev-Zotov, and R. E. Thorne, Phys. Rev. Lett. 74, 5264–5267 (1995).
- ¹⁵¹R. Kurita, M. Koyano, and S. Katayama, Physica B 284–288, 1661–1662 (2000).
- 152S. Kikkawa, M. Koizumi, S. Yamanaka, Y. Onuki, and S. Tanuma, Phys. Status Solidi A 61, K55 (1980).
- ¹⁵³O. Gorochov, A. Katty, N. L. Nagard, C. Levy-Clement, and D. M. Schleich, Mater. Res. Bull. 18, 111–118 (1983).
- 154P.-L. Hsieh, C. M. Jackson, and G. Grüner, Solid State Commun. 46, 505–507 (1983).
- ¹⁵⁵E. Finkman and B. Fisher, Solid State Commun. **50**, 25–28 (1984).
- 156I. G. Gorlova, V. Y. Pokrovskii, S. G. Zybtsev, A. N. Titov, and V. N. Timofeev, JETP Lett. 111, 298–303 (2010).
- 157 I. G. Gorlova, S. G. Zybtsev, and V. Y. Pokrovskii, JETP Lett. 100, 256–261 (2014).
- 1581. G. Gorlovaa, V. Y. Pokrovskii, S. Y. Gavrilkin, and A. Y. Tsvetkov, JETP Lett. 107, 175–181 (2018).
- ¹⁵⁹N. Papadopoulos, E. Flores, K. Watanabe, T. Taniguchi, J. R. Ares, C. Sanchez, I. J. Ferrer, A. Castellanos-Gomez, G. A. Steele, and H. S. J. van der Zant, 2D Mater. 7, 015009 (2019).
- 160 I. G. Gorlova, V. Y. Pokrovskii, A. V. Frolov, and A. P. Orlov, ACS Nano 13, 8495–8497 (2019).
- ¹⁶¹M. Randle, A. Lipatov, A. Kumar, P. A. Dowben, A. Sinitskii, U. Singisetti, and J. P. Bird, ACS Nano 13, 8498–8500 (2019).

- ¹⁶²S. V. Z. Zotov, Phys.-Usp. 47, 533–554 (2004).
- 163 D. V. Borodin, S. V. Zaitsev-Zotov, and F. Y. Nad', Sov. Phys. JETP 66, 793–802 (1987), available at http://www.jetp.ac.ru/cgi-bin/dn/e_066_04_0793.pdf.
- 164 J. McCarten, D. A. DiCarlo, M. P. Maher, T. L. Adelman, and R. E. Thorne, Phys. Rev. B 46, 4456–4482 (1992).
- 165 M. Tsubota, K. Inagaki, T. Matsuura, and S. Tanda, Europhys. Lett. 97, 57011 (2012).
- 166G. Grüner, Rev. Mod. Phys. 60, 1129–1181 (1988).
- 167 J. Kang, W. Liu, D. Sarkar, D. Jena, and K. Banerjee, Phys. Rev. X 4, 031005 (2014).
- ¹⁶⁸A. Allain, J. Kang, K. Banerjee, and A. Kis, Nat. Mater. 14, 1195–1205 (2015).
- 169S. J. Gilbert, A. Lipatov, A. J. Yost, M. J. Loes, A. Sinitskii, and P. A. Dowben, Appl. Phys. Lett. 114, 101604 (2019).
- 170 R. Sun, Y. Gu, G. Yang, J. Wang, X. Fang, N. Lu, B. Hua, and X. Yan, J. Phys. Chem. C 123, 7390-7396 (2019).
- 177 B. L. Al'Tshuler, JETP Lett. 41, 648–651 (1985), available at https://scholar.google.com/scholar?hl=en&q=B.+L.+Al%27tshuler%2C+%22Fluctuations+in+the+Extrinsic+Conductivity+of+Disordered+Conductors%2C%22+Pis%27ma+Zh.+Eskp.+Teor.+Fiz.+41%2C+530-533+%281985%29+%7BJETP+Lett.+41%2C+648-651+%281985%29%7D.
- 1772 P. A. Lee and A. D. Stone, Phys. Rev. Lett. 55, 1622-1625 (1985).
- ¹⁷³P. A. Lee, A. D. Stone, and H. Fukuyama, *Phys. Rev. B* **35**, 1039–1070 (1987).
- ¹⁷⁴Y. Aharonov and D. Bohm, Phys. Rev. 115, 485–491 (1959).
- ¹⁷⁵A. D. Stone, Phys. Rev. Lett. **54**, 2692–2695 (1985).
- 176 R. A. Webb, S. Washburn, C. P. Umbach, and R. B. Laibowitz, Phys. Rev. Lett. 54, 2696–2699 (1985).
- 177 U. Meirav, M. A. Kastner, M. Heiblum, and S. J. Wind, Phys. Rev. B 40, 5871–5874 (1989).
- ¹⁷⁸J. H. F. Scott-Thomas, S. B. Field, M. A. Kastner, H. I. Smith, and D. A. Antoniadis, Phys. Rev. Lett. **62**, 583–586 (1989).
- 179S. B. Field, M. A. Kastner, U. Meirav, and J. H. F. Scott-Thomas, Phys. Rev. B 42, 3523–3536 (1990).
- 180 J. C. Licini, D. J. Bishop, M. A. Kastner, and J. Melngailis, Phys. Rev. Lett. 55, 2987–2990 (1985).
- 181S. W. Stanwyck, P. Gallagher, J. R. Williams, and D. Goldhaber-Gordon, Appl. Phys. Lett. 103, 213504 (2013).
- 182Y. I. Latyshev, O. Laborde, P. Monceau, and S. Klaumünzer, Phys. Rev. Lett.
- **78**, 919–922 (1997).

 183 E. N. Bogachek, I. V. Krive, I. O. Kulik, and A. S. Rozhavsky, Phys. Rev. B **42**, 7614–7617 (1990).
- 184A. S. Pawbake, J. O. Island, E. Flores, J. R. Ares, C. Sanchez, I. J. Ferrer, S. R. Jadkar, H. S. J. van der Zant, A. Castellanos-Gomez, and D. J. Late, ACS Appl. Mater. Interfaces 7, 24185–24190 (2015).
- 185 J. A. Silva-Guillén, E. Canadell, P. Ordejón, F. Guinea, and R. Roldán, 2D Mater. 4, 025085 (2017).
- ¹⁸⁶I. G. Gorlova, A. V. Frolov, A. P. Orlov, V. Y. Pokrovskii, and W. W. Pai, JETP Lett. 110, 417–423 (2019).
- ¹⁸⁷I. Shapir, A. Hamo, S. Pecker, C. P. Moca, O. Legeza, G. Zarand, and S. Ilani, Science 364, 870–875 (2019).